



CrossMark
 click for updates

Cite this: *RSC Adv.*, 2015, 5, 74024

Effect of graphene on the thermophysical properties of melamine-urea-formaldehyde/*N*-hexadecane microcapsules

Bingyang Wu,^{ab} Guo Zheng^{*ab} and Xu Chen^{cd}

Heat transfer performance remains a key factor for the potential application of microencapsulated phase change materials (microPCMs). The purpose of this work is to explore the effect of different amounts of graphene added on the thermophysical properties of microPCMs. Microcapsules containing *n*-hexadecane (C16) with a melamine-urea-formaldehyde (MUF) shell were synthesized by emulsion polymerization. The spectra of Fourier transform infrared spectroscopy (FTIR) confirmed that the MUF shell is fabricated on the surface of C16. Graphene is successfully mixed with microPCMs and the crystal type of microPCMs is not changed, which is detected by X-ray Diffraction (XRD). The results indicated that heat enthalpy of microPCMs gradually decreases with the rising addition of graphene, but the heat transfer performance and thermal stabilities are enhanced. In addition, graphene in microPCMs obviously reduces the degree of supercooling of C16. MicroPCMs with 0.05 wt% added graphene have the best anti-osmosis performance.

Received 29th June 2015
 Accepted 27th August 2015

DOI: 10.1039/c5ra12566a

www.rsc.org/advances

Introduction

In recent years, phase change energy storage materials (phase change materials, PCMs) have become a hot topic in the fields of energy utilization and the material sciences.^{1–3} Phase change energy storage technology efficiently improves the utilization ratio of energy.^{4,5} Microencapsulated phase change materials (microPCMs) have spawned a new research field by taking microcapsule technology and applying it to the phase change materials.⁶ In addition, microPCMs enhance the utilization efficiency of phase change materials and broaden its potential areas of application.⁷ The microencapsulated phase change materials can not only reduce the reaction of the phase change materials and improve the environment to effectively increase the heat transfer area but can also control the volume of phase change materials in phase transition.^{8,9}

MicroPCMs are mainly made of core materials (such as straight-chain alkanes, fatty acids, or composite phase change materials) and wall materials (such as urea-formaldehyde resin,^{10,11} polyurethane¹² and melamine-formaldehyde resin,^{13,14} etc.). Straight-chain alkanes are used as the core material given that it is non-toxic, non-corrosive, and affordable.¹⁵ Organic wall

materials are used in traditional microPCMs. However, the poor thermal conductivity of organic wall materials lead to the low heat absorbing and releasing efficiency of microPCMs, limiting the large-scale application of microPCMs in industry.

Graphene is known as the thinnest material in the world,^{16,17} having a thickness of 0.3354 nm.¹⁸ Electrons face little resistance and interference during electron transmission in graphene layers.^{19,20} The electron mobility of graphene can be achieved $2 \times 10^5 \text{ cm}^2 (\text{V s})^{-1}$ and is about 100 times the electron mobility in silicon with the use of graphene transferring plane semiconductor operations.^{21,22} In addition, the tensile modulus or Young's modulus (1100 GPa) and the ultimate strength (116 GPa) of graphene match single-walled carbon nanotubes.²³ Graphene is light in weight, with good thermal conductivity and contains a large specific surface area.²⁴ Thus, graphene has broad applications due to its excellent properties, and it has broad potential applications in biomedicines,^{25–28} solar cell, sensor, nanoelectronics, high-performance electronic devices, crystallization behavior, field emission materials, gas sensors and energy storage.^{29,30} However, to the best of the author's knowledge, very little work has been done on the application of graphene to microPCMs. Toward this end, microcapsules containing *n*-hexadecane (C16) with melamine-urea-formaldehyde (MUF) shell were synthesized by emulsion polymerization. The surface morphologies of microPCMs were characterized using a field-emission scanning electron microscope (FE-SEM) and optical microscope (BA2000). The crystallographic behaviours of microPCMs were obtained using X-ray diffraction (XRD). The heat transfer performance was measured using the Hot Disk Thermal Constant Analysers. The thermal properties

^aSchool of Material Science and Engineering, Tianjin Polytechnic University, Tianjin, China. E-mail: zhengguo0703@126.com

^bTianjin Engineering Research Center of Textile Fiber Interface Treatment Technology, Tianjin, China

^cKey Laboratory of Advanced Textile Composites, Ministry of Education, Tianjin Polytechnic University, Tianjin, China

^dSchool of Textiles, Tianjin Polytechnic University, Tianjin, China

of microPCMs were investigated by differential scanning calorimetry (DSC) and thermal gravimetric analysis (TGA).

Experimental

Materials

N-Hexadecane (C16) used as core material was purchased from Alfa Aesar, USA. Melamine (M) (Sigma-Aldrich, USA), urea (U) (Sigma-Aldrich, USA) and formaldehyde solution, 37 wt% in H₂O (F) (Sigma-Aldrich, USA) were used as shell materials. Sodium dodecyl sulfate (SDS) and polyvinyl alcohol (PVA) used as emulsifying agents were obtained from Guangzhou Tehsun Chemical Technology Co., Ltd, China. Graphene (thickness: 1.0–1.77 nm; layers: 1–5; specific area: 360–450 m² g⁻¹) was obtained from Suzhou Hengqiu Graphene Science and Technology Co., Ltd, China.

Preparation of the MicroC16

MicroC16 were synthesized by emulsion polymerization. A mixture of melamine and formaldehyde aqueous solution with distilled water was heated at 70 °C for 20 min until a clear

melamine-formaldehyde (MF) prepolymer solution was obtained. This mixture was subsequently cooled down to room temperature (RT = 25 °C). Urea was added into the MF prepolymer solution until complete dissolution, which was melamine-urea-formaldehyde (MUF) pre-polymer solution. Graphene was dispersed in an aqueous solution of SDS and PVA in a certain proportion. The solution was mildly sonicated for 30 min using an ultrasonic cleaner to obtain stable graphene suspension. Herein the SDS functioned as the surfactant reducing the surface tension of the aqueous solution and assisting in graphene dispersion; the PVA functioned as a stabilizer, inhibiting the reunion of graphene in the solution. By adding C16 and graphene suspension to the beaker of the MUF pre-polymer solution, the reaction solution was dispersed by the XHF-D type high speed disperser for 20 min to a form stable oil-in-water (O/W) emulsion. Subsequently, the reaction beaker was removed into the 80 °C water bath and allowed to react for 4 h. The obtained suspension solution of microPCMs was washed with distilled water to remove unreacted polymers and C16 after the suspension was placed for 24 h. Finally, microPCMs were obtained with vacuum filtration. Reaction conditions were shown in Table 1; the schematic fabrication of the microPCMs and the fabricated process of the microcapsule shell at the surface of C16 droplets was shown in Fig. 1.

Table 1 Reaction conditions

Reagent (wt%)	MicroC16	MicroC16 ₁	MicroC16 ₂	MicroC16 ₃
Graphene	—	0.05	0.1	0.2
C16	7.6	7.6	7.6	7.6
Melamine	2.4	2.4	2.4	2.4
Formaldehyde	4.5	4.5	4.5	4.5
Urea	0.8	0.8	0.8	0.8
PVA	0.4	0.4	0.4	0.4
SDS	1.2	1.2	1.2	1.2
Distilled water	83.1	82.05	82.0	81.9

Characterization

Fourier transformed infrared (FTIR) spectra of C16 and microPCMs were obtained using an FTIR spectroscopy (TENSOR37 Bruker, Germany) in the range of 4000–500 cm⁻¹ at room temperature. The surface morphologies of microPCMs containing different amounts of graphene added were characterized using a field-emission scanning electron microscope (FE-SEM, S-4800 Hitachi, Japan) and optical microscope (BA2000) obtained by Chongqing Photoelectric Instrument Co.,

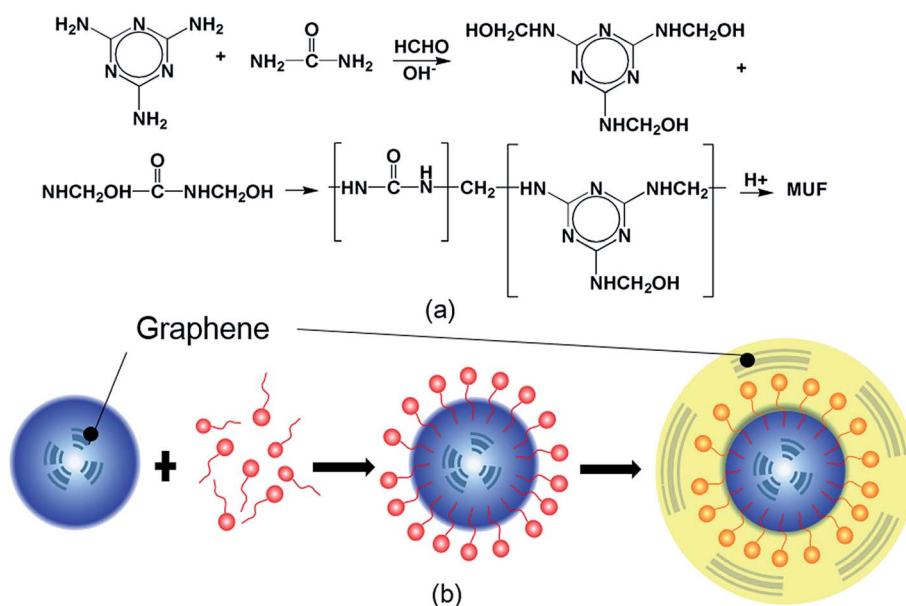


Fig. 1 Schematic formation of the graphene microPCMs based on *n*-hexadecane core and MUF resin shell by emulsion polymerization.

Ltd, China. The diameters of the microcapsules were measured on the OM micrographs, and more than 200 microcapsules were counted. The diffraction patterns of C16, graphene and microPCMs were obtained using an X-ray diffractometer (XRD, D8 Bruker, Germany, 40 kV, 150 mA) at 0 °C, with the scanning range at 5–40°. The thermal conductivity coefficient and thermal diffusivity of microPCMs containing different amounts of graphene added were measured by using the Hot Disk Thermal Constant Analysers (TPS-2500S Hot Disk, Sweden) at room temperature. The phase change properties of the C16 and microPCMs were measured using a Differential Scanning Calorimetry (DSC, 200-F3 NETZSCH, Germany) in the range of –10–60 °C at a rate of ± 10 °C min⁻¹ in a nitrogen atmosphere. Thermal stability of C16 and the prepared microPCMs with different amounts of graphene added were investigated using a thermogravimetric analyzer (TGA, STA449F3 NETZSCH, Germany) at a scanning rate of 10 °C min⁻¹ in the range of 25–600 °C in a nitrogen atmosphere. The anti-osmosis measurements of microPCMs were characterized in 0.96 g ml⁻¹ density ethyl alcohol by means of a 723PC spectrophotometer obtained by Shanghai Cany Precision Instrument Co., Ltd, China.

Results and discussion

Chemical characterization

The FTIR spectrums of C16 and microPCMs are shown in Fig. 2(a). This figure shows that the peaks at 2910 and 2850 cm⁻¹ present at –CH₂ stretching vibration. The peaks at 1469 cm⁻¹ present –CH₃ asymmetric bending vibration. The peak at 2910 and 2850 cm⁻¹ are not obvious in the curve (c) of Fig. 2, compared with curve (a). This reflects that the coating effect of microPCMs for the core material is excellent. A wide and strong absorption peak is observed at 3404 cm⁻¹, which is formed with the N–H and O–H stretching vibration peak superposition (combination). The peak at 1562 cm⁻¹, and the peak at 813 cm⁻¹ collectively reflects the triazine ring bending characteristic and presents the C=N stretching vibration. The C–H stretching vibration peak is found at 1342 cm⁻¹. The peak at 1161 cm⁻¹ represents the C–O–C stretching vibration. Alcohols C–O stretching vibration peak appears near the 1015 cm⁻¹. As seen in the curve (b) of Fig. 3, the peaks at 1620 and 1440 cm⁻¹ present C=C stretching vibration, and C=C is formed by the reduced graphene oxide. The characteristic peak in the curve (d) and (c) of Fig. 2 is not found near the 1720 cm⁻¹, which indicates an absence of C=O in microPCMs. The results of FTIR show that the ether bond is formed by a polycondensation reaction of methylol melamine in prepolymer, which illustrates the formation of cross-linked prepolymer.

Morphology of microPCMs

Optical and FE-SEM micrographs of MicroC16, MicroC16₁, MicroC16₂ and MicroC16₃ are shown in Fig. 3. As shown in Fig. 3(a)–(d), microPCMs are spherical and have uniform size. It can be clearly seen that the graphene is successfully coated in microPCMs. In addition, the content of graphene in microPCMs increased with the rising addition of graphene. FE-SEM

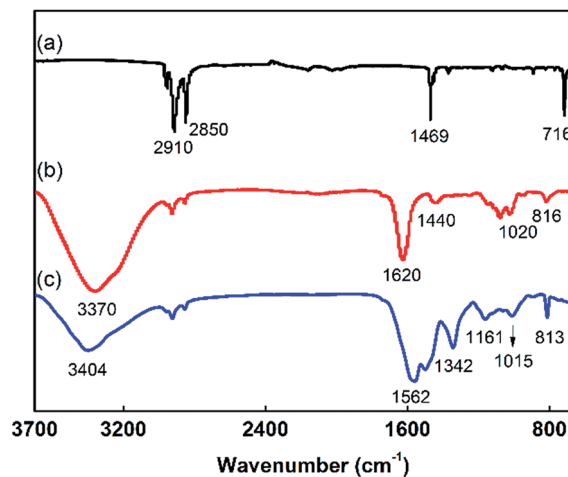


Fig. 2 FTIR spectra of C16 and microPCMs: (a) C16; (b) graphene microPCMs; (c) pure microPCMs.

micrographs of microPCMs (Fig. 3(e)–(h)) showed that the surfaces of microPCMs without graphene were relatively rough and adhered to many irregular MUF polymers particles. Moreover, microPCMs surfaces were increasingly smooth and irregular particles were significantly reduced with the rising addition of graphene. The reason is that graphene in solution hinders the self-aggregation of MUF pre-polymers in the reaction solution, thus forming smooth surfaces of microPCMs. However, the larger autopolymer particles on the surface of microPCMs were observed as the amount of graphene added continued to increase to 0.2 wt%. This is because the graphene adhered to each other, providing a nucleating agent for MUF pre-polymers when the graphene concentration in the solution reached a certain level. This led to polymerization and precipitation of pre-polymers in the solution.

In addition, C16 was solidified and exothermic when the environmental temperature was below the freezing point of C16, accompanied by obvious microPCMs volume change. This change made the microPCMs wall unsmooth. This phenomenon explained that the C16 were successfully encapsulated into the microPCMs, and the microPCMs shell had excellent elasticity and toughness. Therefore, it would not burst due to the core material phase change. Particle size distributions of microPCMs are shown in Fig. 3(i)–(l). The particle size distribution of MicroC16 is relatively concentrated and the average particle size is 9.85 μ m. Particle size distribution of microPCMs with the rising addition of graphene is broadened and the average particle size decreases slightly. Taken together, the morphology of microPCMs is the most ideal and particle size distribution is relatively uniform with 0.05–0.1 wt% graphene addition.

Crystallography

The X-ray diffraction patterns of C16, graphene, MicroC16, MicroC16₁, MicroC16₂ and MicroC16₃ are shown in Fig. 4. Both the C16, graphene, and microPCMs are highly crystallized, given that the MUF copolymer shell of microPCMs is amorphous,³¹ it is convenient to analyze the crystallographic forms of

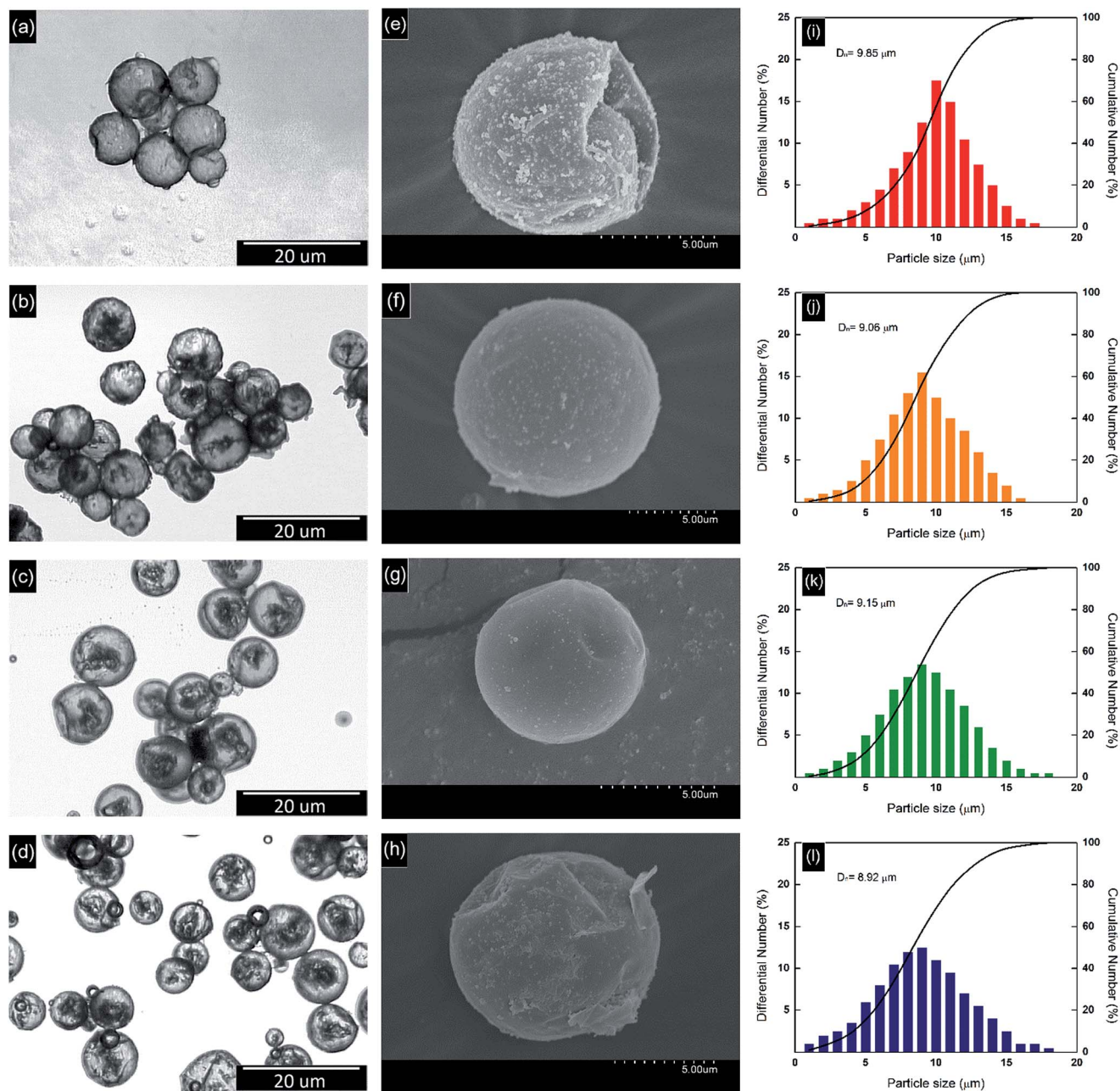


Fig. 3 Optical micrographs, FE-SEM images and particle size distribution of (a, e and i) MicroC16, (b, f and j) MicroC16₁, (c, g and k) MicroC16₂ and (d, h and l) MicroC16₃.

encapsulated C16. The XRD pattern of C16 shows four characteristic peaks of triclinic (010), (011), (100), and (111), as observed in the pattern of all samples at 19.2° , 19.6° , 23.3° and 24.7° , which are the characteristic peaks of C16, respectively.³² XRD pattern shows that there are characteristic peaks of graphene at 2θ of 26.6° in XRD curve of graphene, MicroC16₁, MicroC16₂ and MicroC16₃, indicating that graphene is mixed with the microPCMs. The crystal structure of the C16 in the microPCMs is the same as that of the C16. Nevertheless, the intensities in the diffractions patterns at the low 2θ (5 to 15°) decreased dramatically after the microencapsulation. These findings indicate that the small space of the microPCMs

inhibits the motion of the C16 chains to some extent, resulting in a decrease of the crystallinity. The crystallization peak position of MicroC16₁, MicroC16₂ and MicroC16₃, compared with MicroC16, does not indicate migration. This demonstrates that the addition of graphene has no remarkable impact on the crystal type of microPCMs.

Heat transfer performance

Fig. 5 illustrates that the heat transfer performance of microPCMs with different amounts of graphene added at room temperature. The thermal conductivity coefficient and thermal

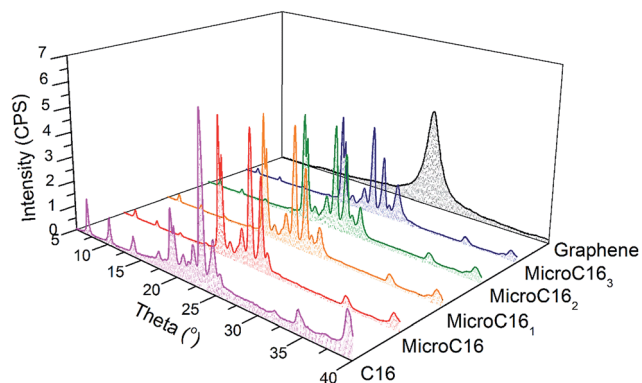


Fig. 4 XRD patterns of C16, graphene, MicroC16, MicroC16₁, MicroC16₂ and MicroC16₃.

diffusivity of microPCMs are dramatically increased with the rising addition of graphene, since the graphene has excellent thermal conductivity properties and can effectively reduce the thermal resistance of wall material, thus enhance the heat transfer performance of microPCMs. However, the change rate (K) of thermal conductivity and thermal diffusivity of microPCMs are reduced ceaselessly, namely, that the heat transfer property lifting range of microPCMs decreases gradually with the increasing graphene added. The explanation for this is that the excessive graphene is free in solution and cannot be completely mixed into microPCMs with the high concentration of graphene in the solution. Thermal conductivity coefficient and thermal diffusivity of microPCMs are $0.053 \text{ W m}^{-1} \text{ K}^{-1}$ and $0.238 \text{ m}^2 \text{ s}^{-1}$, respectively. The coefficient of thermal conductivity and thermal diffusivity of microPCMs adding 0.1 wt% graphene are $0.154 \text{ W m}^{-1} \text{ K}^{-1}$ and $0.56 \text{ m}^2 \text{ s}^{-1}$. The coefficient of thermal conductivity and thermal diffusivity of graphene microPCMs, compared with pure microPCMs, are increased by 191% and 160%, respectively. Thus, it can be seen that adding a small amount of graphene can remarkably improve the heat transfer performance of microPCMs.

Empirical models of addition, thermal diffusivity and coefficient of thermal conductivity of graphene can be established, respectively. It can be more intuitive performance quantitative relationship of the two through the model. We use the quadratic function model to approximate the functional relationship between them:

$$y = K + a_1x + a_2x^2, x \in (0, +\infty) \quad (1)$$

where y is dependent variable, x is addition of graphene, K is constant term, a_1 and a_2 are control coefficient, the following functions are obtained by curve fitting:

$$y = 0.28 + 2.42x - 3.76x^2, x \in (0, +\infty) \quad (2)$$

$$y = 0.09 + 1.04x - 0.43x^2, x \in (0, +\infty) \quad (3)$$

As shown in eqn (2) and (3), y is positively correlated with x when x is small. y is negatively correlated with x when x is small. As shown in Table 2, the F test values of two fitting results are

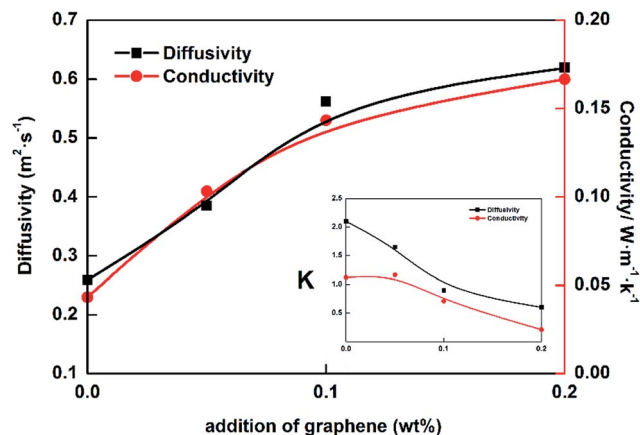


Fig. 5 Heat transfer performance of microPCMs with different amounts of graphene added.

171.23 and 105.08, respectively, which indicates that the two models have high fitting precision. The value of Sig. is less than 0.05 at the level of 95% confidence interval, which shows that addition of graphene is significantly related to the thermal diffusivity and thermal conductivity of graphene.

Phase change property

The phase change properties of the C16, MicroC16, MicroC16₁, MicroC16₂ and MicroC16₃ are investigated by DSC, and their thermograms are displayed in Fig. 6. The melting and crystallization properties of all the samples are obtained from DSC analysis and summarized in Table 3. As can be seen from Fig. 6(a), there is a significant decrease in enthalpy of the prepared microPCMs with different amounts of graphene added in comparison to those of the C16. This is likely due to the phase change behaviors confined by the inner space of the microPCMs. It is also notable that the crystallizing behavior of microPCMs varies with the rising addition of graphene. For MicroC16, two crystallization peaks, α and β are observed from the DSC cooling thermograms. This is because the microencapsulation of phase change materials is coated in a small space, the crystallization converts into homogeneous crystallization, and the degree of supercooling increases. Furthermore, the phase change heat can not be released at once, and the crystallization process must be finished by releasing heat multiple many times. The peak α decreases gradually and its shoulder shifts towards higher temperature with the rising addition of graphene because of the excellent thermal performance of graphene. Dispersed graphenes are added into

Table 2 Model summary and parameter estimates

Fitting parameter	Model summary			Parameter estimates		
	R Square	F	Sig.	Constant	a_1	a_2
Diffusivity	0.99	171.23	0.02	0.28	2.42	-3.76
Conductivity	0.99	105.08	0.03	0.09	1.04	-0.43

microPCMs wall and core material with poor thermal conductivity to accelerate the phase change heat transfer. In addition, the graphene in the microPCMs plays the function of the nucleating agent during the phase change process of the core material so as to make the crystallization of internal core material change from homogeneous crystallization to the heterogeneous crystallization.

The phase change property of microPCMs can be described with three parameters: encapsulated efficiency (η) and phase change temperature T_c and T_m , which can be determined by means of DSC analysis. The enthalpies of microPCMs from solid-liquid phase change are important physical properties affecting the working effect of the microPCMs, which strongly depends on the encapsulated efficiency of PCMs. Moreover, η can be calculated by the enthalpies obtained from DSC curves, based on the formulation given below:

$$\eta = \frac{\Delta H_{m,\text{microPCMs}} + \Delta H_{c,\text{microPCMs}}}{\Delta H_{m,\text{PCMs}} + \Delta H_{c,\text{PCMs}}} \quad (4)$$

where η is the microencapsulation ratio of C16; $\Delta H_{m,\text{microPCMs}}$ and $\Delta H_{c,\text{microPCMs}}$ are melting enthalpy and crystallization enthalpy of microPCMs; $\Delta H_{m,\text{PCMs}}$ and $\Delta H_{c,\text{PCMs}}$ are melting enthalpy and crystallization enthalpy of *n*-alkane mixture, respectively. The results indicated that the thermal properties of the as-prepared microPCMs were satisfactory for energy storage applications.

Thermal stability

Thermogravimetry (TG) diagrams and differential thermal gravity (DTG) were shown in Fig. 7(a) and (b). As can be seen from Fig. 7(a), the C16 starts to lose weight at about 145 °C and completes at about 270 °C. The weight losing processes of microencapsules contains three steps. The first step, the weight loss of microPCMs occurs at 70 °C, which is due to the fact that residual moisture in microPCMs is lost through drying. The second step is from 210 to 230 °C, which is caused by the decomposition of C16. The third step is from 430 to 460 °C

Table 3 Phase change properties of C16 and microPCMs with different amounts of graphene added

Sample	T_m (°C)	ΔH_m (J g ⁻¹)	T_c (°C)		ΔH_c (J g ⁻¹)	η (%)
			α	β		
C16	15.2	199.6	—	—	198.4	—
MicroC16	14.7	167.4	7.7	2.1	169.8	84.7
MicroC16 ₁	15.9	154.2	10.7	6.4	155.3	77.8
MicroC16 ₂	15.8	136.5	—	—	138.3	69.1
MicroC16 ₃	14.6	104.7	—	—	103.6	52.2

because of further thermal decomposition of microPCMs wall. Weight loss of C16 in microPCMs has obvious delay, compared with pure C16, which shows that the capsule wall block volatilization of C16. Consequently the thermal stability of microPCMs is improved. As can be seen from 250–300 °C and 450–500 °C of Fig. 7(b), the mass attenuation rate of microPCMs slightly declines and the thermal stability enhances slightly with the rising addition of graphene, which is because graphene has good heat transfer performance and makes the heat distribution in the microPCMs more uniform, thereby improving the thermal stability of microPCMs.

Anti-osmosis property

The anti-osmosis property is an important feature in the application of microPCMs. Anti-osmosis measurement was used to evaluate the sealing performance of microPCMs wall. Fig. 8 shows the release rates of microPCMs prepared by using graphene, indicating that there is a significant influence of the graphene content on microPCMs release behaviors. It can be seen that the anti-osmosis property of Sample MicroC16₁ is optimal, since a small amount of graphene added can reduce auto-polymerization of the MUF pre-polymers in the reaction solution to make the microcapsule wall more smooth and firm. However, the anti-osmosis property of microcapsule is poor with the rising addition of graphene. Osmosis rate of MicroC16₃

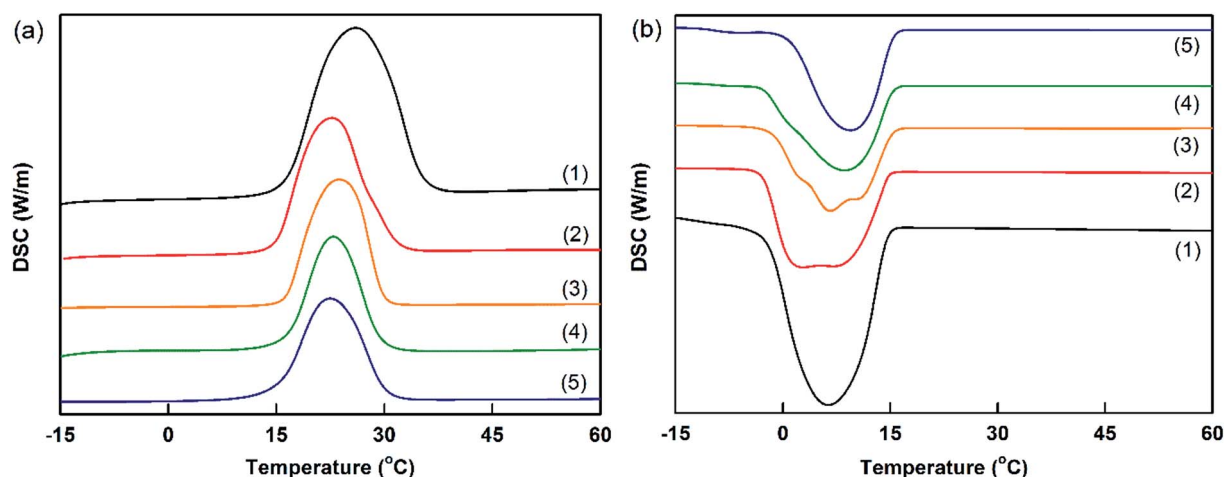


Fig. 6 DSC thermograms of C16(1), MicroC16(2), MicroC16₁(3), MicroC16₂(4) and MicroC16₃(5): (a) heating thermograms, and (b) cooling thermograms.

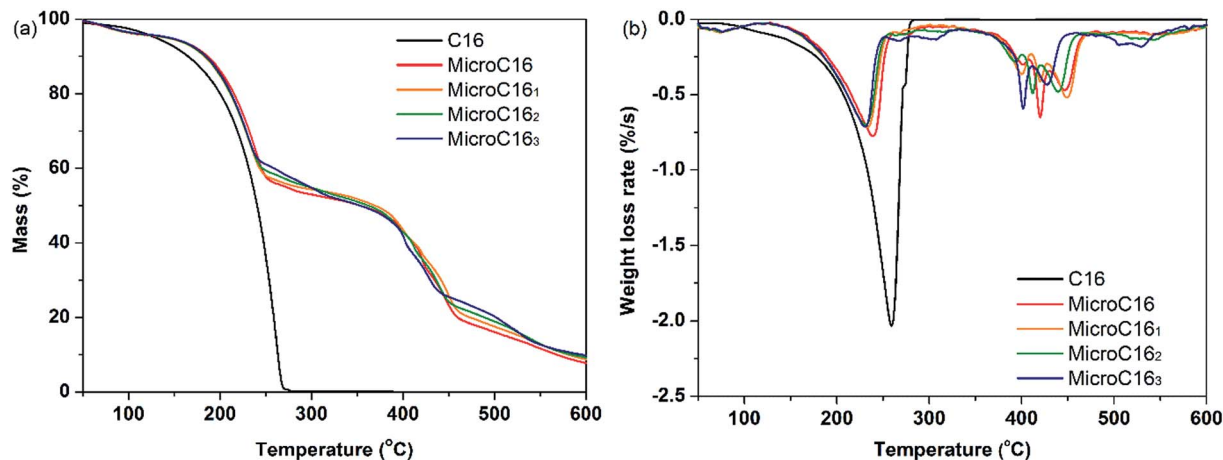


Fig. 7 TG spectra of C16, MicroC16, MicroC16₁, MicroC16₂ and MicroC16₃: (a) TG and (b) DTG curves.

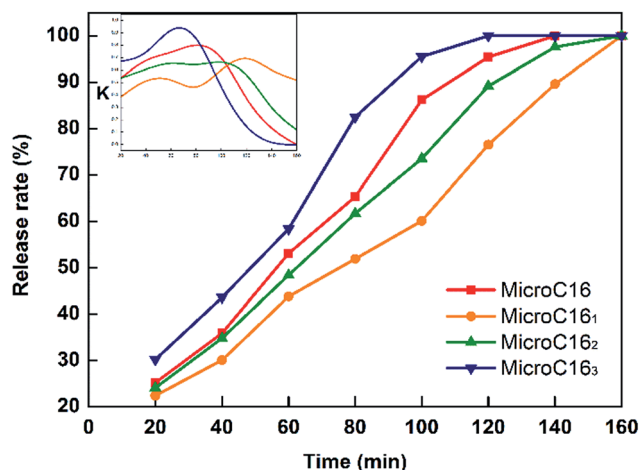


Fig. 8 Release curves of MicroC16, MicroC16₁, MicroC16₂ and MicroC16₃.

was obviously accelerated and the anti-osmosis property had fallen dramatically. The reason is that adding too much graphene into the reaction system created too much graphene which could destroy the evenness of the MUF resin in the microPCMs wall, bringing about bad encapsulation of microPCMs shell. In a word, the anti-osmosis property of microPCMs was increased to some extent when the addition of graphene was 0.05 wt%. However, the anti-osmosis property of microPCMs declined gradually with the rising addition of graphene.

Conclusions

Novel microcapsules containing C16 as core material and MUF polymer as shell material and graphene were synthesized by emulsion polymerization. MicroPCMs have a relatively spherical shapes with the 0.05–0.1 wt% graphene. The addition of graphene has no remarkable impact on the crystal type of microPCMs, and the crystal structure of the C16 in the

microPCMs is similar to that of the C16. In addition, the heat transfer performance, thermal stabilities and anti-osmosis performance of microPCMs have the most remarkable improvement. In summary, the addition of graphene endowed microPCMs with enhanced features and expanded the potential fields of application and scope of microPCMs. With the improvement of the graphene preparation technology and the growth of production, graphene microPCMs will play a more important role in the future.

Acknowledgements

The authors would especially like to thank Tianjin Research Program of Application Foundation and Advanced Technology (NO. 15JCZDJC38400) and the National Natural Science Foundation of China (NO. 51303131).

Notes and references

- 1 D. Wu, B. Ni, Y. J. Liu, S. Chen and H. L. Zhang, *J. Mater. Chem. A*, 2015, **3**, 9645–9657.
- 2 D. Wu, W. Wen, S. Chen and H. L. Zhang, *J. Mater. Chem. A*, 2015, **3**, 2589–2600.
- 3 S. B. Ye, Q. L. Zhang, D. D. Hu and J. C. Feng, *J. Mater. Chem. A*, 2015, **3**, 4018–4025.
- 4 X. Y. Huang, Z. P. Liu, W. Xia, R. Q. Zou and R. P. S. Han, *J. Mater. Chem. A*, 2015, **3**, 1935–1940.
- 5 H. Zhang, L. M. Liu and W. M. Lau, *J. Mater. Chem. A*, 2013, **1**, 10821–10828.
- 6 X. L. Qiu, L. X. Lu and Z. Z. Chen, *J. Appl. Polym. Sci.*, 2015, **17**, 41880–41888.
- 7 D. Z. Yin, H. Liu, L. Ma and Q. Y. Zhang, *Polym. Adv. Technol.*, 2015, **6**, 613–619.
- 8 Y. Zhang, X. D. Wang and D. Z. Wu, *Sol. Energy Mater. Sol. Cells*, 2015, **133**, 56–68.
- 9 A. Sari, C. Alkan, D. K. Döğücü and Ç. Kızıl, *Sol. Energy*, 2015, **115**, 195–203.
- 10 W. Li, X. X. Zhang, X. C. Wang and J. J. Niu, *Mater. Chem. Phys.*, 2007, **106**, 437–442.

- 11 C. Z. Xin, Y. C. Tian, Y. W. Wang and X. A. Huang, *Text. Res. J.*, 2013, **8**, 831–839.
- 12 J. Y. Kwon and H. D. Kim, *Fibers Polym.*, 2006, **7**, 12–19.
- 13 J. F. Su, L. X. Wang and L. Ren, *J. Appl. Polym. Sci.*, 2006, **101**, 1522–1528.
- 14 D. Z. Yin, L. Ma and W. C. Geng, *Int. J. Energy Res.*, 2015, **39**, 661–667.
- 15 G. Sun and Z. Zhang, *Int. J. Pharm.*, 2002, **242**, 307–311.
- 16 R. T. Weitz and A. Yacoby, *Nat. Nanotechnol.*, 2010, **5**, 699–700.
- 17 M. Mitra, C. Kulsi, K. Chatterjee, K. Kargupta, S. Ganguly, D. Banerjee and S. Goswamid, *RSC Adv.*, 2015, **5**, 31039–31048.
- 18 C. Lee, X. Wei, J. W. Kysar and J. Hone, *Science*, 2008, **321**, 385–388.
- 19 A. K. Geim, *Science*, 2009, **324**, 1530–1534.
- 20 A. K. Geim and K. S. Novoselov, *Nat. Mater.*, 2007, **6**, 183–191.
- 21 X. Zhang, H. T. Zhang and C. Li, *RSC Adv.*, 2014, **4**, 45862–45884.
- 22 J. S. Wu, W. Pisula and K. Mullen, *Chem. Rev.*, 2007, **107**, 718–747.
- 23 M. J. Allen, V. C. Tung and R. B. Kaner, *Chem. Rev.*, 2010, **110**, 132–145.
- 24 D. Li, G. H. Li and P. F. Lv, *RSC Adv.*, 2015, **5**, 30602–30609.
- 25 K. Yang, L. Z. Feng, X. Z. Shi and Z. Liu, *Chem. Soc. Rev.*, 2013, **42**, 530–547.
- 26 H. C. Zhang, G. Grünerbe and Y. L. Zhao, *J. Mater. Chem. B*, 2013, **1**, 2542–2567.
- 27 J. Liu, Y. R. Huang, A. Kumar, A. Tan, S. B. Jin, A. Mozhi and X. J. Liang, *Biotechnol. Adv.*, 2014, **32**, 693–710.
- 28 L. Cheng, C. Wang, L. Z. Feng, K. Yang and Z. Liu, *Chem. Rev.*, 2014, **114**, 10869–10939.
- 29 D. F. Li, Y. Y. Liu and H. X. Ma, *RSC Adv.*, 2015, **5**, 31670–31676.
- 30 M. Mitra, C. Kulsi and K. Chatterjee, *RSC Adv.*, 2015, **5**, 31039–31048.
- 31 H. Z. Zhang and X. D. Wang, *Colloids Surf., A*, 2009, **332**, 129–138.
- 32 E. B. Sirota and A. B. Herhold, *Science*, 1999, **283**, 529–532.